JOURNAL OF SPACECRAFT AND ROCKETS
Vol. 30, No. 3, May–June 1993

Aerodynamic Effects of Body Roughness

Asher Sigal*
Technion—Israel Institute of Technology, Haifa 32000, Israel

A modular model of a slender tangent-ogive-cylinder body having an interchangeable centerbody was tested alone and in combination with a set of four fins or with a flare at Mach numbers of 0.8 and 2.4. The baseline centerbody was smooth. One centerbody was knurled and three were roughened by square threads of fixed height and of various pitch-to-height ratios. Centerbody roughness increased the normal-force-curve slope and shifted the center of pressure rearward for bodies alone and for body-flare combinations. In the case of the finned configurations, roughness caused small changes in the normal-force-curve slope and the center-of-pressure location. Qualitatively, the changes observed at the subsonic Mach number were the same as those at the supersonic Mach number.

Nomenclature

A = parameter in Eq. (4)
AB = afterbody
B = centerbody
C_f = average rough-wall skin-friction coefficient
C_{f_0} = average smooth-wall skin-friction coefficient
C_m = pitching-moment coefficient
C_N = normal-force coefficient
C_{N_α} = normal-force-curve slope
C_{X_0} = zero-lift axial-force coefficient, base contribution excluded
D = centerbody diameter, reference length
D_B = diameter of flare base
H = boundary-layer shape factor
h = height of roughness element
h_{es} = height of equivalent sand roughness
l = length
M = Mach number
N = nose
P = pressure
p = pitch of threads
Re_D = Reynolds number based on centerbody diameter
S_B = wetted area of centerbody
S_R = reference area, $\pi D^2/4$
T = temperature
U = freestream velocity
u_τ = friction velocity
X_{cp} = center-of-pressure location measured from nose tip
α = angle of attack
δ^* = boundary-layer displacement thickness
δ^{**} = boundary-layer momentum thickness
θ = flare angle
λ = pitch-to-height ratio, p/h
μ = coefficient of viscosity
ν = kinematic viscosity
ρ = density
τ = wall friction stress

Subscripts

t = stagnation conditions
w = wall value
∞ = freestream

Received June 22, 1990; presented as Paper 90-2850 at the AIAA Atmospheric Flight Mechanics Meeting, Portland, OR, Aug. 20–22, 1990; revision received Feb. 20, 1992; accepted for publication Nov. 25, 1992.

*Associate Professor, Faculty of Aerospace Engineering. Associate Fellow AIAA.

Introduction

SEVERAL types of artillery projectiles feature circumferential roughness. In particular, kinetic energy penetrators are accelerated in the barrel by a sabot. The transfer of the accelerating force from the sabot to the projectile is obtained by threads or grooves. From an aerodynamic point of view, these mechanical devices can feature a large degree of surface roughness.

The addition of roughness to bodies is expected to cause three aerodynamic effects. The first and obvious one is an increase in the axial force. The second effect is an increase in the contribution of the body to the normal force, due to the increased displacement thickness of the boundary layer. The third effect is a reduction in the efficiency of stabilizers (when present), due to the masking effect of the thick boundary layer.

In spite of the increasing interest in this area of ballistics, no systematic studies of these effects were found in the open literature.

The objective of the present study is to experimentally explore the expected effects of roughness on a slender ogive-cylinder body alone and in combination with two types of stabilizers: fins and a flare.

Models, Tests, and Facility

Configurations

The baseline configuration was a smooth tangent-ogive-cylinder body having a nose fineness ratio of 3.5 and a cylinder fineness ratio of 10.0. The outer diameter was 40 mm. The cylinder was divided into an 8.0 caliber centerbody and a 2.0 caliber afterbody. An outline of the test configurations and the designation of the parts are shown in Fig. 1. One stabilizer consisted of a cruciform set of fins having a span-to-diameter ratio of 2.0. The aspect ratio of the fins was 1.35, the taper ratio was 0.3, and the trailing edge was unswept. The fins were mounted on a cylindrical afterbody. The second stabilizer was a conical flare having a base diameter to reference diameter ratio of 1.5. Four rough centerbodies, all having a roughness element height of 0.5 mm, were tested. One was diamond knurled and the pyramidal roughness elements had a pitch of 2.0 mm and width of 1.0 mm. The second one was a square thread with a pitch of 1.0 mm. The third and fourth ones were series of circumferential square ridges having pitches of 2.0 and 4.0 mm, respectively. The height of 0.5 mm was selected to assure that the axial-force increment, due to the roughness, will be considerably larger than the experimental uncertainty. The square cross section of three roughness configurations was selected because of the availability of data on the equivalent sand roughness, which enables analytical predictions. The geometry of the roughness elements is shown in Fig. 1.

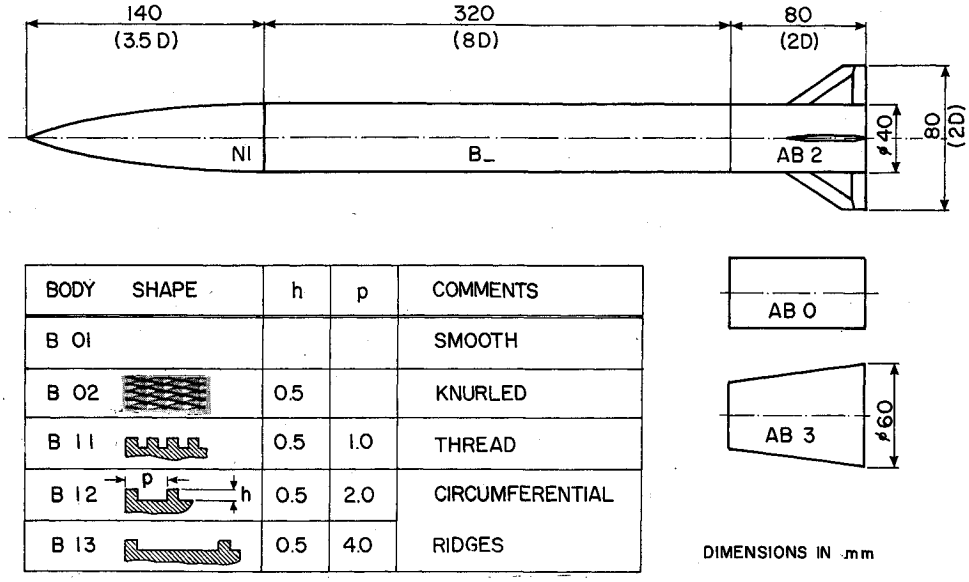

Fig. 1 Outline of the wind-tunnel model and designation of the modules.

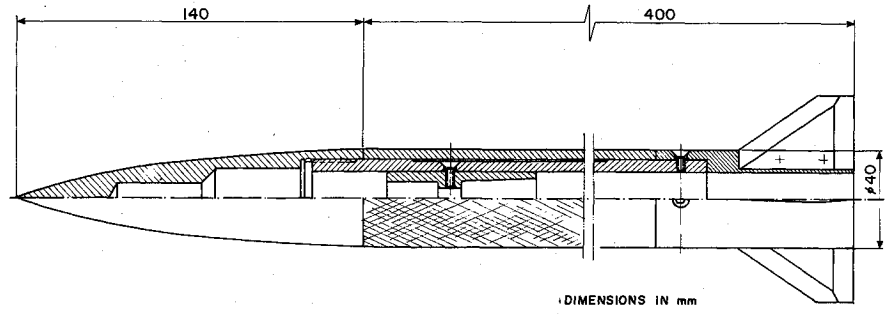

Fig. 2 General assembly of the finned model, configuration *N*1.*B*02.*AB*2.

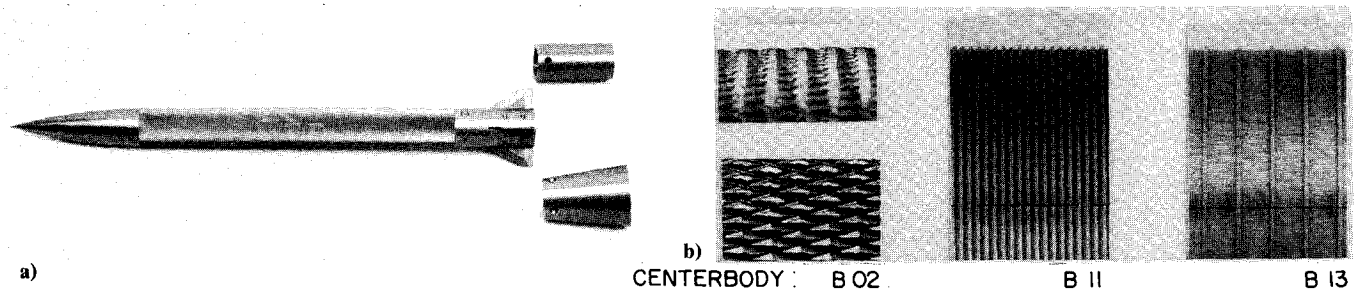

Fig. 3 Photographs of the model: a) configuration *N*1.*B*02.*AB*2; and b) details of centerbodies *B*02, *B*11, and *B*13.

Wind-Tunnel Model

The wind-tunnel model had a modular construction to facilitate the interchange of centerbodies. The afterbody was attached to a central stem. The centerbodies slid on the stem and were secured by the nose. A general assembly of the finned configuration is shown in Fig. 2. Photographs of the same model and of details of centerbodies *B*02, *B*11, and *B*13 are shown in Fig. 3.

The knurling tool for the manufacturing of centerbody *B*02 was made by the Swiss toolmaker DOSS. It has two cutting wheels with 1.0-mm division that are mounted on 30-deg oblique pivots.

Wind Tunnels

The experiments were carried out in the two high-speed wind tunnels of the Aeronautical Research Center of the Technion. The transonic facility is a closed-cycle, injection-type tunnel capable of operating at Mach numbers up to 1.16. The test section is 60 cm wide by 80 cm high, and the floor and the ceiling are perforated. For details see Salomon et al.[1] The supersonic tunnel is of the blowdown type. The test section is 40 cm wide by 50 cm high, and the flexible nozzle covers Mach numbers from 1.5 to 4.0. The supersonic facility was described by Kadushin and Rom.[2]

The test conditions are summarized in Table 1. The angle of attack varied from -5 to $+5$ deg. The rates of change of the angles of attack were about 1 deg/s in the transonic tunnel and about 2 deg/s in the supersonic one.

Measurements

A six-component sting balance was used for the measurement of forces and moments. The base pressure was measured by two independent probes mounted on both sides of the sting. The difference in the reading of the two transducers was

Table 1 Test conditions

M	P_t, N/cm^2	T_t deg, K	Re_D, $\times 10^6$
0.8	10.1	276	0.45
2.4	51.0	276	3.4

Table 2 Comparison of results of the baseline configuration with Barth's data base[2]

Mach number:	0.8	2.4
C_{N_α}		
Present	2.47	2.72
Barth	2.43	2.72
Δ	1.6	—
X_{cp}/D		
Present	3.47	1.85
Barth	3.45	2.08
Δ	0.02	0.23

small enough so that only one was used for data reduction. A schlieren system was used to visualize the flow.

Test Results

Axial Force

The base pressure was strongly affected by the sting balance and did not represent free-flight conditions. The base drag contribution was therefore subtracted from the total drag, and only the difference is considered. The zero-lift axial-force coefficient is shown in Fig. 4a. The drag increments due to the knurls and the dense square threads of centerbodies $B02$ and $B11$ are similar. An increase in the pitch of the ridges increased the axial-force increment. For the finned configurations, the increments in the axial-force coefficient due to roughness are similar to those of the body alone.

Normal Force and Center of Pressure

The normal-force-curve slope and the center-of-pressure location were obtained by fitting straight lines to the linear sections of C_N vs α and C_m vs C_N data, respectively. The results are shown in Figs. 4b and 4c. In the case of the body alone, configurations $N1.B\text{-}.AB0$, centerbody roughness increased the normal-force-curve slope and shifted the center of pressure rearward, relative to the smooth centerbody case. In the case of the finned models, configurations $N1.B\text{-}.AB2$, the normal-force-curve slope changed only slightly by centerbody roughness, indicating the masking effect of the thickened boundary layer on the fins. The phenomenon is apparent at both the subsonic and the supersonic Mach numbers. The three-dimensional roughness caused a small forward shift of the center of pressure. The dense two-dimensional roughness, centerbody $B11$, did not change the center of pressure location relative to the smooth body case. In the cases of the more sparse roughness, the center of pressure shifted slightly aft. In the case of the flared models, configurations $N1.B\text{-}.AB3$, the normal-force-curve slope increased and the center of pressure shifted aft with an increase in roughness, except for the knurled centerbody where changes in these characteristics were very small.

Validation of the Results

The smooth centerbody results were compared with existing databases. The results of the smooth body alone, configuration $N1.B01.AB0$, were compared with those of Barth.[3] The comparison is summarized in Table 2.

The difference in the normal-force-curve slope is 1.6% at $M = 0.8$ and null at $M = 2.4$. The difference in the center-of-pressure location is only 1.7% of body length at $M = 2.4$ and very small at $M = 0.8$.

The contribution of the smooth-body flare to the normal-force-curve slope was obtained by subtracting C_{N_α} of the smooth body alone from that of the flared configuration. The results were normalized by $2[(D_B/D)^2 - 1]$, the analytical prediction by slender-body theory. The results are compared in Fig. 5 with data bases of Refs. 4–7 that were compiled by Sigal et al.[7] The present results fall within the scatter of the data.

The two comparisons validate the accuracy of the results.

Analysis

Effects of Roughness

The effects of roughness on the normal-force-curve slope and the zero-lift axial-force coefficient were extracted from the data using

$$\Delta C_{N_\alpha} = C_{N_\alpha}(N1.B - .ABi) - C_{N_\alpha}(N1.B01.ABi)$$
$$\Delta C_{X_0} = C_{X_0}(N1.B - .ABi) - C_{X_0}(N1.B01.ABi) \quad (1)$$

where $i = 1$ for body alone, $i = 2$ for the finned configuration, and $i = 3$ for the flared configuration. The results are shown in the two parts of Fig. 6. The increment in the normal-force-curve slope due to centerbody roughness of the flared body is larger than that of the body alone. In the case of the finned configuration, the effect of roughness depends on the orientation of the fins in roll. The masking effect in the + position is smaller than that in the x position.

For the case of a rough body alone, Sigal and Danberg[8] related the change in the normal-force-curve slope to a contri-

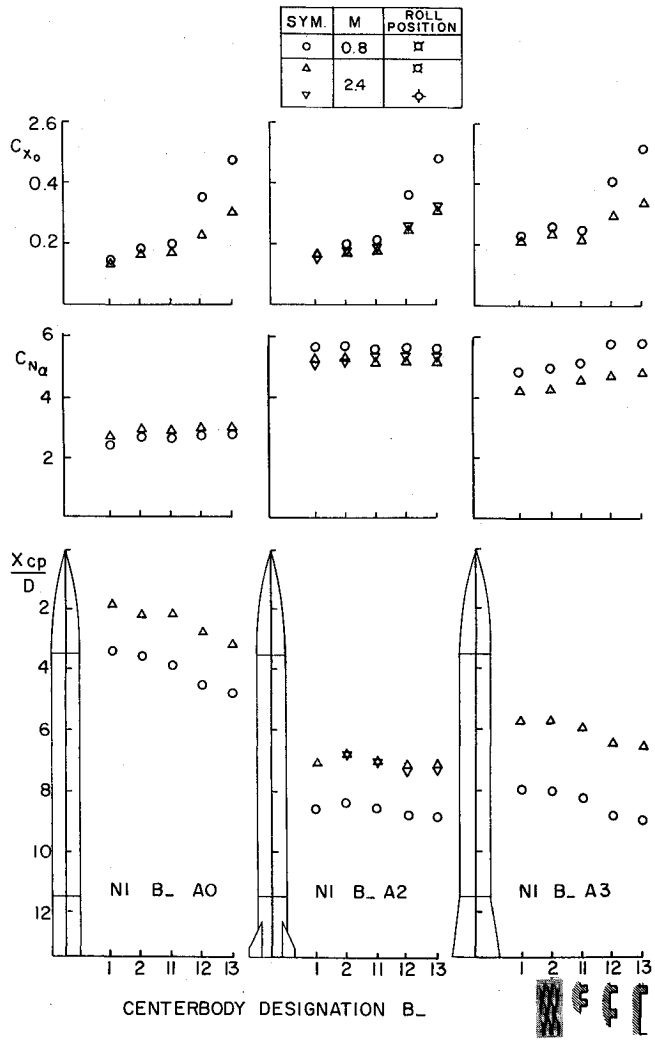

Fig. 4 Summary of test results: a) axial-force coefficient, b) normal-force-curve slope, and c) center-of-pressure location.

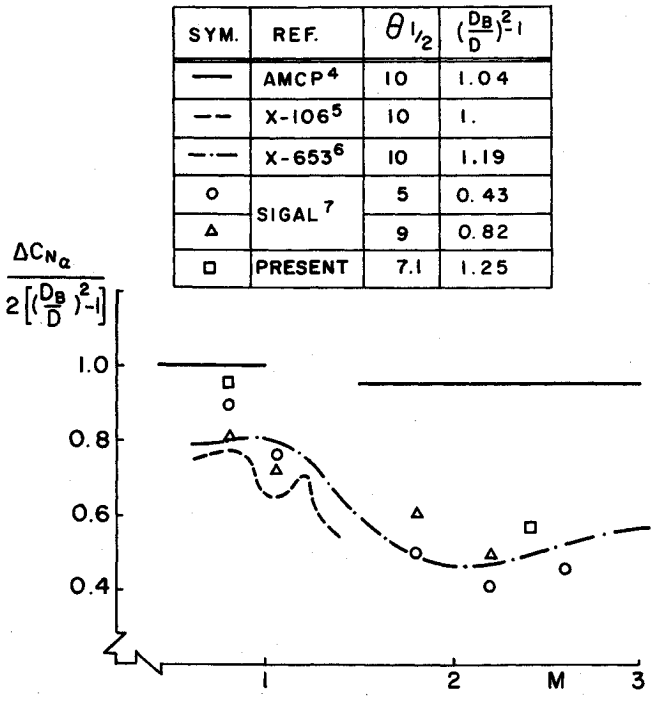

Fig. 5 Comparison of the contribution of the flare to the normal-force-curve slope with other sources.

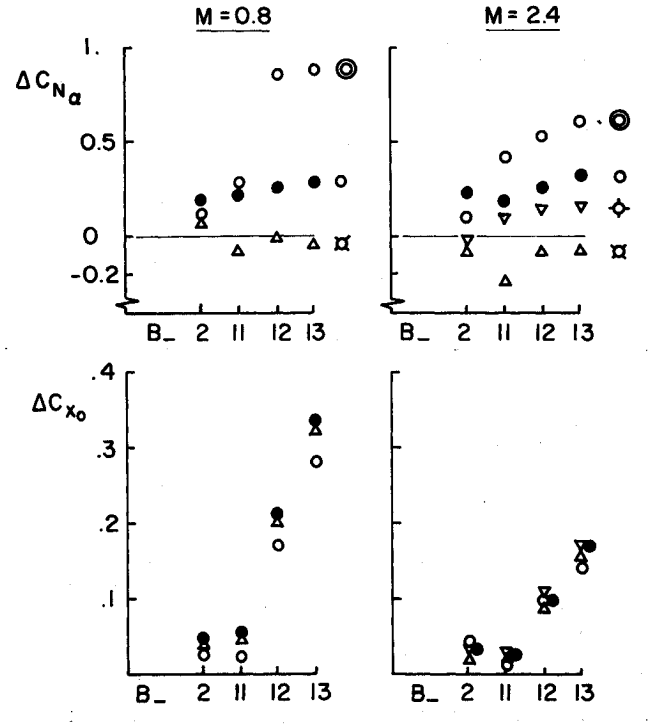

Fig. 6 Effect of centerbody roughness on a) normal-force-curve slope, and b) axial-force coefficient.

bution of an effective flare, created by the displacement of the thickened boundary layer. The same approach is used by Ref. 9 in a methodology for the evaluation of the effect of Reynolds number on the stability derivatives of smooth bodies. According to Ref. 8,

$$\Delta C_{N_\alpha} = 8\frac{\Delta\delta^*}{D}$$

and

$$\Delta\delta^{**} = \frac{D}{8}\Delta C_{X_0}$$

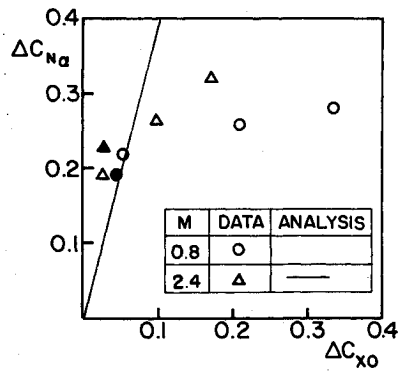

Fig. 7 Relationship between the body-alone changes in the normal-force-curve slope and the axial-force coefficient.

Table 3 Equivalent sand roughness

Centerbody	λ	h_{es}/D
*B*11	2	0.00122
*B*12	4	0.0371
*B*13	8	0.1

Assuming that the boundary-layer shape factor is not affected by roughness and that

$$\frac{\Delta\delta^*}{\Delta\delta^{**}} = \frac{\delta^*}{\delta^{**}} = H$$

one obtains

$$\Delta C_{N_\alpha} = H\Delta C_{X_0}$$

The changes in the body-alone characteristics were obtained by setting $i = 1$ in Eq. (1). The relationship between ΔC_{N_α} and ΔC_{X_0} is shown in Fig. 7. For the tests at $M = 0.8$, transition on the smooth body took place on the centerbody. Hence, only the tests at $M = 2.4$, where the boundary layer is mostly turbulent, were analyzed. For this Mach number it was found from Ref. 10 that $H = 3.85$. The analytical prediction for the dependence of ΔC_{N_α} on ΔC_{X_0}, for $M = 2.4$, is also shown in Fig. 7. The experimentally obtained data show a near-linear dependence, with a slope that is much smaller than the predicted slope. We suppose that the discrepancy between test data and analysis is a result of the shedding of circumferential vortices, entrapped between ridges, at angle of attack. This effect reduces the buildup of displacement thickness and the associated ΔC_{N_α}.

Axial Force Due to Square Ridges

The increments in the axial-force coefficient due to the series of square ridges, centerbodies *B*11, *B*12, and *B*13, were estimated using the method developed by Danberg and Sigal.[11] The method is based on a new correlation of the equivalent sand roughness.[12] For two-dimensional roughness composed of equally spaced square ridges, this correlation gives:

$$\frac{h_{es}}{h} = \begin{cases} 0.003215\lambda^{4.925}, & 1.4 \le \lambda \le 4.89 \\ 8.0 \quad\quad\quad , & 4.89 < \lambda < 13.25 \\ 151.71\lambda^{-1.1379}, & 13.25 \le \lambda \le 100.0 \end{cases} \tag{2}$$

In the present case, $h = 0.5$ mm. Table 3 shows the normalized equivalent sand roughness.

The amplification of the skin friction, which is the ratio of rough-wall to smooth-wall skin-friction coefficients, is based on an empirical correlation, taken from Ref. 4:

$$\frac{C_f}{C_{f_0}} = 0.11 + 0.89 \log \frac{h_{es}u_\tau}{\nu_w} \tag{3}$$

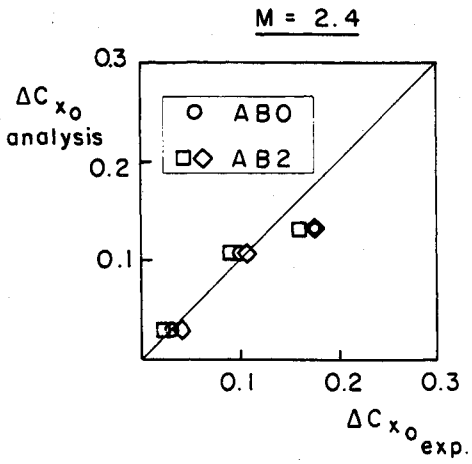

Fig. 8 Comparison between analytically and experimentally obtained increments in the axial-force coefficient due to roughness.

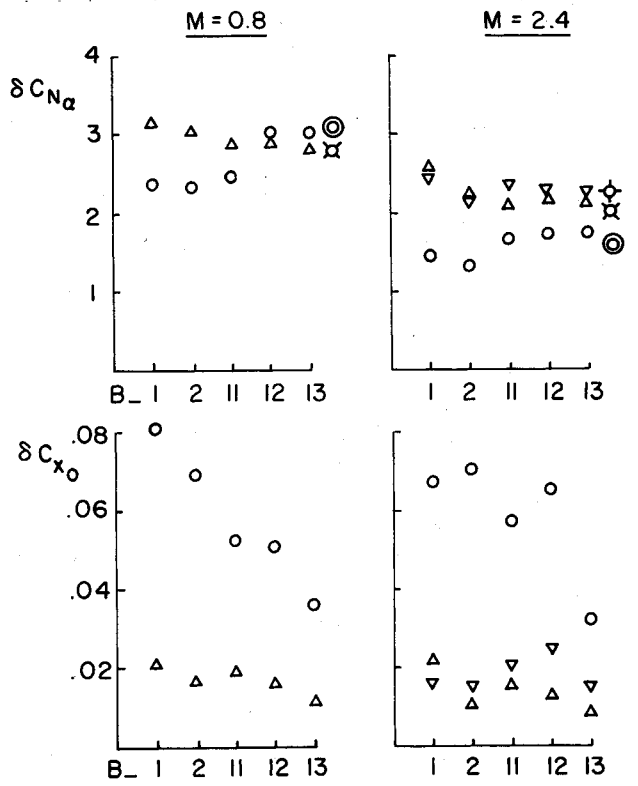

Fig. 9 Contribution of the stabilizers to a) normal-force-curve slope, and b) axial-force coefficient.

Using the definition of friction velocity $u_\tau = \sqrt{\tau/\rho_w}$, and assuming a constant pressure across the boundary layer, this expression can be written as

$$\frac{C_f}{C_{f_0}} = 0.11 + 0.89 \log\left[\frac{h_{es}}{D}\sqrt{\frac{C_f}{2}} A(M) Re_D\right] \tag{4}$$

where

$$A(M) = \frac{1}{(\mu_w/\mu_\infty)(T_w/T_\infty)^{1/2}}$$

Because of the short duration of the tests, it was assumed that the wall temperature equals the room temperature.

The average smooth-wall skin-friction coefficient was estimated, using Ref. 10, to be 0.0017 at $M = 2.4$. The rough-wall skin-friction coefficient was found using Eq. (4), and the increment in the axial-force coefficient is related to it by

$$\Delta C_{X_0} = (S_B/S_R)(C_f - C_{f_0}) \tag{5}$$

For the reason mentioned in the preceding section, only the tests at $M = 2.4$ were analyzed. A comparison between predicted and experimentally obtained values of ΔC_{X_0} is presented in Fig. 8. For centerbodies $B11$ and $B12$, the agreement is very good. In the case of $B13$, the analysis underpredicts the experimentally obtained value by 15%.

Effect of Body Roughness on the Stabilizers

The contributions of the stabilizers to the normal-force-curve slope and to the zero-lift axial-force coefficient were derived by

$$\begin{aligned}\delta C_{N_\alpha} &= C_{N_\alpha}(N1.B - .ABi) - C_{N_\alpha}(N1.B - .AB0)\\ \delta C_{X_0} &= C_{X_0}(N1.B - .ABi) - C_{X_0}(N1.B - .AB0)\end{aligned} \tag{6}$$

where $i = 2$ for the fins and $i = 3$ for the flare. The results are presented in the two parts of Fig. 9.

The contribution of the fins to the normal-force-curve slope is decreased by body roughness. The magnitude of this change is close to the increase in the body-alone contribution due to roughness ΔC_{N_α}, which is shown in Fig. 6a. The contribution of the flare is increased by circumferential roughness and is slightly decreased by the knurled centerbody. These changes are accompanied by appropriate changes in the center-of-pressure location.

In spite of the scatter in δC_{X_0}, it seems that the contribution of the fins is independent of body roughness. In the case of the flare, δC_{X_0} decreases with an increase in roughness.

Qualitatively, the effects of body roughness on the aerodynamic characteristics at the subsonic Mach number are the same as in the supersonic case.

Summary and Conclusions

The aerodynamic effects of body roughness were experimentally investigated at Mach numbers of 0.8 and 2.4. The baseline configuration was a smooth tangent-ogive-cylinder body with overall fineness ratio of 13.5. Four interchangeable rough centerbodies were also tested with the body alone and in combination with a set of four fins or with a flare.

Centerbody roughness increased the normal-force-curve slope and shifted the center of pressure rearward for bodies alone and for body-flare combinations. In the case of the body-fins combination, centerbody roughness caused only small changes in the normal-force coefficients. This finding indicates that the reduction in the contribution of the fins to the normal force due to centerbody roughness is similar to the increment of the contribution of the body.

The increment in axial-force coefficient due to roughness caused by a series of square ridges was well predicted by the method developed by Danberg and Sigal.

The increment in body alone normal-force-curve slope, due to centerbody roughness, was not proportional to the increment in the axial-force coefficient, as predicted. Additional tests are needed to establish a relationship between these two parameters for a wide range of roughness configurations.

Acknowledgments

This study was supported by the M. and A. Albert Fund for Research and Development in Aeronautical Engineering. Wind-tunnel tests were provided by the Aerodynamics Laboratory of the Aeronautical Research Center. D. Weihs and A. Seginer encouraged and supported the research. The wind-tunnel engineer was M. Victor. The seeds of this study were sowed during the author's residence at the U.S. Army Ballistic Research Laboratory as a National Research Council Research Associate.

References

[1]Salomon, M., Bracha, J., and Rom,J., "Characteristics of the 60 cm × 80 cm Induction Driven Close Return Transonic Wind Tunnel at the Aeronautical Research Center," *Israel Journal of Technology,* Vol. 8, Nos. 1-2, March 1970, pp. 111-118.

[2]Kadushin, I., and Rom, J., "Design of an Intermittent, Single Jack Flexible Nozzle Supersonic Wind-Tunnel for Mach Numbers 1.5 to 3.5," Technion, TAE Rept. 86, Haifa, Israel, July 1968.

[3]Barth, H., "The Normal Force, Center of Pressure and Tangential Force Characteristics of Slender Nose-Cylinder Configurations at Mach Numbers Between 0.8 to 4.0," MBB Corp., Rept. UA 137-73, Munich, Germany, 1973.

[4]Anon., "Design of Aerodynamically Stabilized Free Rockets," U.S. Army Material Command, AMCP 706-280, 1968.

[5]Wakefield, R.M., Knechtel, E.D., and Treon, S.L., "Transonic Static Aerodynamic Characteristics of a Blunt Cone-Cylinder Body with Flared Afterbodies of Various Angles and Base Areas," NASA TM X-106, 1959.

[6]Jorgensen, L.H., Spahr, J.R., and Hill, W.A., Jr., "Comparison of the Effectiveness of Flares with That of Fins for Stabilizing Low-Fineness-Ratio Bodies at Mach Numbers from 0.6 to 5.8," NASA TM X-653, May 1952.

[7]Sigal, A., Yaacobi, A., and Avital, G., "The Effect of Afterbody Geometry on the Aerodynamic Characteristics of Circular Bodies," AIAA Paper 87-0444, Jan. 1987.

[8]Sigal, A., and Danberg, J.E., "Aerodynamic Analysis of Solid Fuel Ramjet Projectiles," U.S. Army Ballistic Research Lab., Memorandum Rept. BRL-MR-3687, Aberdeen Proving Ground, MD, May 1988.

[9]Anon., "Normal-Force-Curve and Pitching-Moment-Curve Slopes of Forebody-Cylinder Combinations at Zero Angle of Attack for Mach Numbers Up to 5," Engineering Sciences Data Unit International, Item 89008, London, April 1989.

[10]Anon., "The Compressible Two-Dimensional Turbulent Boundary Layer with Application to Wedges, Cylinders and Cones," Engineering Sciences Data Unit International, Item 68020, London, March 1968.

[11]Danberg, J. E., and Sigal, A., "Analysis of Turbulent Boundary-Layer Over Rough Surfaces with Application to Projectile Aerodynamics," U.S. Army Ballistic Research Lab., Technical Rept. BRL-TR-2977, Aberdeen Proving Ground, MD, Dec. 1988.

[12]Sigal, A., and Danberg, J.E., "New Correlation of Roughness Density Effect on the Turbulent Boundary Layer," *AIAA Journal,* Vol. 28, No. 3, 1990, pp. 554-556.